JOC Article

Experimental and Theoretical Studies of Fused-Ring Persistent [1,2,4]Thiadiazinyl Radicals†

Józef Zienkiewicz‡ and Piotr Kaszynski*

Organic Materials Research Group, Department of Chemistry, Vanderbilt University, Nashville, Tennessee 37235

Victor G. Young Jr.

X-ray Crystallographic Laboratory, Department of Chemistry, University of Minnesota, Twin Cities, Minnesota 55455

piotr.kaszynski@vanderbilt.edu

Received July 30, 2004

Five persistent radicals **1a**−**1e** were generated by the oxidation of 4*H*-[1,2,4]thiadiazines **2a**−**2e** and studied with ESR and UV−vis spectroscopy. Three of the radicals, **1a**, **1d**, and **1e**, were generated in high yields (>90%) using either SO_2Cl_2/amine in toluene or AgO/K_2CO_3 in a toluene/MeCN mixture. Halogenated radicals **1d** and **1e** were sufficiently stable for chromatographic isolation and vacuum sublimation. The solution stability of the fluorinated **1d** was measured at $t_{1/2} \approx 4$ months in the absence of oxygen, and **1e** at $t_{1/2} \approx 40$ min in the presence of air. The crystal and molecular structures of **1d** were determined by X-ray crystallography showing columns of parallel almost evenly spaced planar heterocycles connected by infinite ···N···S··· chains. Cyclic voltammetry of **1d** and **1e** shows reversible reduction waves at about 0 V and irreversible oxidations at about 1.2 V. Spectral and electrochemical properties of **1** were well reproduced by DFT methods.

Introduction

There is continuous interest in stable free radicals as components of organic magnetic materials[1] and molecular conductors.[2] In this context, we have been investigating π-delocalized heterocyclic radicals as possible structural elements for liquid crystals[3,4] to study electric and magnetic properties of free radicals in organized media. Recently, we demonstrated the significant chemical stability of three- and four-ring heterocycles[5] and thus suitability for functionalization to form discotic mesogens. Our earlier attempt to develop a thiatriazinyl radical system suitable for construction of calamitic liquid crystals was unsucessful.[6] Therefore, we focused on benzo[1,2,4]thiadiazinyl and its derivatives, which upon proper substitution at the 3 and 7 positions can form molecules with elongated shapes conducive to the formation of liquid crystalline phases.[7]

Scant literature data shows that four persistent partially chlorinated benzo[1,2,4]thiadiazinyls were generated by oxidation of the corresponding 4*H*-thiadiazines[8] or reduction of the appropriate sulfiminyl chlorides.[8,9] The radicals were reported to persist for 24 h in solution in the presence of air, but their isolation was not attempted. Despite poucity of data, the reported stability was encouraging and prompted us to investigate this general class of [1,2,4]thiadiazinyls.

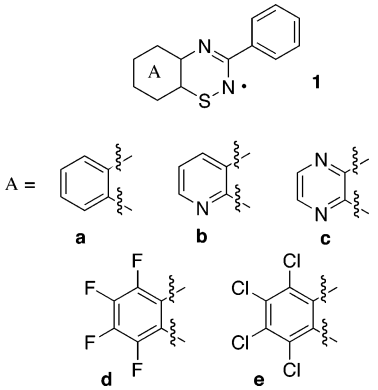

Initially, we have concentrated on the evaluation of stability of the radicals as a function of the ring structure and finding an efficient method for their generation and isolation. Thus, we investigated parent 3-phenylbenzo-

* To whom correspondence should be addressed. Ph: (615) 322-3458. Fax (615) 343-1234.

† Dedicated to Prof. Josef Michl on the occasion of his 65th birthday.

‡ On leave from University of Wroclaw, Poland.

(1) Rawson, J. M.; Palacio, F. In *π-Electron Magnetism. From Molecules to Magnetic Materials*; Veciana, J., Ed.; Springer: New York, 2001; Vol. 100, pp 93−128 and references therein.

(2) Barclay, T. M.; Cordes, A. W.; Haddon, R. C.; Itkis, M. E.; Oakley, R. T.; Reed, R. W.; Zhang, H. *J. Am. Chem. Soc.* **1999**, *121*, 969−976 and references therein.

(3) Kaszynski, P. In *Magnetic Properties of Organic Materials*; Lahti, P. M., Ed.; Marcel Dekker: New York, 1999; pp 305−324.

(4) Patel, M. K.; Huang, J.; Kaszynski, P. *Mol. Cryst. Liq. Cryst.* **1995**, *272*, 87−97.

(5) Benin, V.; Kaszynski, P. *J. Org. Chem.* **2000**, *65*, 8086−8088.

(6) Farrar, J. M.; Patel, M. K.; Kaszynski, P.; Young, V. G., Jr. *J. Org. Chem.* **2000**, *65*, 931−940.

(7) Demus, D. In *Handbook of Liquid Crystals*; Demus, D., Goodby, J. W., Gray, G. W., Spiess, H.-W., Vill, V., Eds.; Wiley-VCH: New York, 1998; Vol. 1, pp 133−187.

10.1021/jo0486746 CCC: $27.50
Published on Web 10/07/2004

TABLE 1. Methods, Maximum Yields, and Optimum Times for Generation of Radicals 1 by Oxidation of 2

	max yield[a] (time)				
method	**a**	**b**	**c**	**d**	**e**
A: PbO_2/K_2CO_3; benzene	26% (25 min)	38% (30 min)	2% (105 min)	10% (40 min)	7% (60 min)
B: AgO/K_2CO_3; benzene	29% (30 min)	46% (35 min)	5% (120 min)	13% (50 min)	11% (80 min)
C: AgO/K_2CO_3; MeCN/toluene 1:1	94% (1.5 min)[b]	2% (5 min)	<2%	96% (1.5 min)[c]	91% (1.5 min)[c]
D: SO_2Cl_2/pyridine; toluene	98%	0%	0%	93%[c,d]	86%[c,d]

[a] Maximum concentration established by ESR. [b] Maximum yield estimated by UV spectroscopy. ESR analysis shows 74% of the radicals after 10 min. [c] ESR analysis of isolated solid. [d] In some experiments $EtMe_2N$ was used instead of pyridine.

SCHEME 1

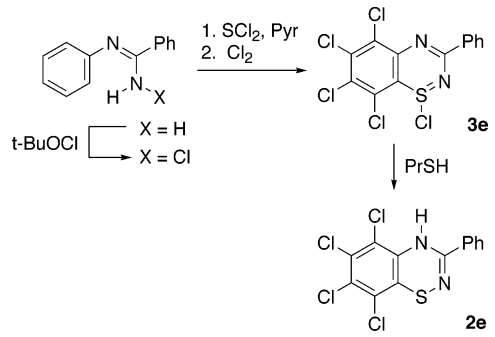

[1,2,4]thiadiazinyl (**1a**) and the effect of incorporation of nitrogen atoms (**1b** and **1c**) and also tetrafluorination (**1d**) and tetrachlorination (**1e**)[9] of the fused benzene ring on the radical stability. Keeping in mind the synthetic constraints posed by the precursors and challenges in the isolation of the pure liquid crystalline radicals, we focused solely on oxidation of the corresponding 4*H*-[1,2,4]thiadiazines with inorganic oxidants to generate the radicals.

Here we describe the generation of five radicals **1a**−**1e** by oxidation of the corresponding [1,2,4]thiadiazines and isolation and extensive characterization of **1d** and **1e**. Subsequently, we report their spectroscopic characterization (UV−vis and ESR) and electrochemical behavior aided by DFT calculations. In the context of our interest in radicals **1** as structural elements of liquid crystalline materials, we also report extensive studies of the generation methods for the radicals and their chemical stability.

Results

Synthesis. The preparation of thiadiazines **2a**−**2d** is reported elsewhere.[10] The tetrachloro analogue **2e** was prepared in about 38% overall yield using adaptations of literature methods (Scheme 1).[9,11] Thus, reduction of crude sulfiminyl chloride **3e** with dry 1-propanethiol gave thiadiazine **2e** in about 84% yield. The use of 1-propanethiol instead of 4-ClC_6H_4SH used for a related system[11] significantly simplified purification of the thiadiazine. The chloride **3e** was obtained according to a literature procedure by insertion of SCl_2 into *N*-chloro-*N*′- phenylbenzamidine in the presence of pyridine followed by exhaustive chlorination with Cl_2.[9]

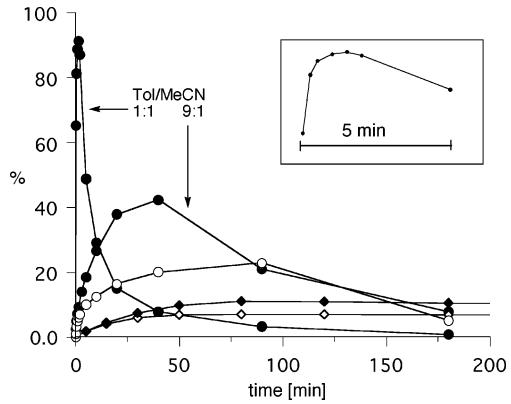

FIGURE 1. Formation of **1e** by oxidation of **2e** with AgO/K_2CO_3 (filled symbols) and PbO_2/K_2CO_3 (open symbols) in benzene (diamonds) and MeCN/toluene (circles) followed by ESR (diamonds) or intensity of absorption at 680 nm (circles). The inset shows the initial 5 min of **2e** oxidation with AgO/K_2CO_3 in MeCN/toluene 1:1 mixture.

Generation and Isolation of Radicals. Generation of radicals by oxidation of **2** was investigated under several conditions (Scheme 2), and the results are shown in Table 1. Initially, a 10- to 20-fold excess of PbO_2 (Method A) or AgO (Method B)[12] in the presence of K_2CO_3 was used in dry benzene. The oxidation reactions were generally slow, and the maximum concentration of the radical was reached after about 30−90 min (Table 1 and Figure 1). AgO was found to be a generally more effective oxidant than PbO_2. The highest yield of the radical, about 46%, was observed by ESR for the pyrido derivative **1b**, and the lowest spin concentrations were recorded for the pyrazino derivative **1c** (5%). The halogenated radicals **1d** and **1e** were generated in a maximum yield of about 10% after about 1 h. Interestingly, the log of the observed spin yields correlate with the calculated enthalpy of N−H homolytic bond dissociation in the 4*H*-thiadiazines **2**.[13] In each case a significant amount of starting thiadiazine **2** remained unreacted. Using larger amounts of oxidant and base (up to 50 equiv) had an insignificant effect on the spin yield of **1e**. No **1a** was detected when Et_3N was used as a base.

When benzene was replaced with MeCN or with a 1:1 mixture of MeCN/toluene in oxidations of **2** with AgO/K_2CO_3 (Method C), the rate of radical generation was markedly improved but the decomposition rate was also higher (Figure 1). The rapid (under 2 min) and almost quantitative generation of the radicals was observed only for thiadiazine derivatives **2a**, **2d**, and **2e**. The nitrogen-

(8) Markovskii, L. N.; Talanov, V. S.; Polumbrik, O. M.; Shermolovich, Y. G. *Russ. J. Org. Chem.* **1981**, *17*, 2338−2339.
(9) Shermolovich, Y. G.; Simonov, Y. A.; Dvorkin, A. A.; Polumbrik, O. M.; Borovikova, G. S.; Kaminskaya, E. I.; Levchenko, E. S.; Markovskii, L. N. *Russ. J. Org. Chem.* **1989**, *25*, 550−553.
(10) Zienkiewicz, J.; Kaszynski, P.; Young, V. G., Jr. *J. Org. Chem.* **2004**, *69*, 2551−2561.
(11) Levchenko, E. S.; Borovikova, G. S.; Borovik, E. I.; Kalinin, V. N. *Russ. J. Org. Chem.* **1984**, *20*, 176−181.
(12) AgO was used in generation of iminoxyl radicals: Jezierski, A. *Magn. Reson. Chem.* **1989**, *27*, 130−133.
(13) Kaszynski, P. *Molecules* **2004**, *9*, 000.

SCHEME 2

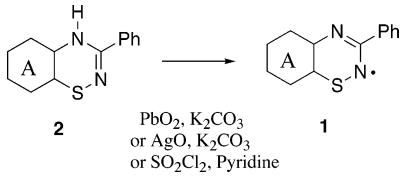

containing heterocyclic radicals **1b** and **1c** were generated in trace quantities under these conditions, and rapid formation of a brown-red-colored species was observed. Oxidation of **2b** and **2c** with AgO or PbO_2 in the absence of base gave low concentrations of the corresponding radicals. For instance, **1b** was generated in about 12% max yield after about 10 min, and **1e** was observed in 60% yield after about 5 min. The use of PbO_2 instead of AgO or much less MeCN (e.g., 1:9 MeCN/toluene) was significantly less effective and the reaction was slow and incomplete as tested for **1e**.

Analysis of the time-dependent spin concentration curves using a kinetic equation for two consecutive reactions[14] showed that the rate of radical formation k_f is about 1×10^{-3} s^{-1} using Methods A and B and over an order of magnitude faster when Method C is used. The rate of radical decomposition (k_d) is slower by a factor ranging between 3 for **1a** to over 100 for **1d** and **1e** with Methods A and B and about 30 with Method C. The curve fitting also shows that the maximum yields for the radicals in the first two methods are moderate at best, reaching about 50% for **1b**, while Method C gives close to quantitative yields of **1a**, **1d**, and **1e**.

In an attempt to develop an alternative method for generation of radicals, we investigated the reaction of **2** with SO_2Cl_2. After optimization of the reaction conditions, it was found that simultaneous dropwise addition of solutions of 0.5 equiv of SO_2Cl_2 and 1 equiv of pyridine or Me_2EtN to solutions of **2** gives the corresponding benzo[1,2,4]thiadiazinyl derivatives **1a**, **1d**, and **1e** in reproducible high spin yields of about 90% (Table 1, Method D). In contrast, no radical formation was detected for the pyridio and pyrazino derivatives **1b** and **1c**.

Other oxidants such as $K_3Fe(CN)_6$ or $K_2S_2O_8$ used in aqueous−benzene or solid phase−benzene phase transfer catalysis systems (Bu_4NBr) were ineffective in the case of **1b**, and only slow accumulation of decomposition products was observed.

The high efficiency of generation of benzo[1,2,4]-thiadiazine radicals (**1a**, **1d**, and **1e**) and acceptable yields for **1b** prompted us to investigate the isolation of the four radicals in the solid state. Thus, cold solutions of radicals generated using Methods C or D (Table 1) were passed through short Florisil columns at −78 °C under a flow of nitrogen. A solution of radical **1a** partially decolorized upon filtration and completely bleached after 10−15 min at about 0 °C. The pyridio radical **1b**, generated using Method B, was more stable than **1a** and could be isolated as a solid containing about 20% of the original spin (by solution ESR measurement).

The halogenated radicals **1d** and **1e** showed significantly higher stability. The reaction mixtures could be filtered through Florisil even at ambient temperature under nitrogen and concentrated giving the solid radicals in high yields. Both of the halogenated radicals were obtained as black-green solids, which could be stored in a freezer under an inert atmosphere for several weeks without detected decomposition. The spin concentration measured after dissolving the solid samples indicated about 90% purity of the radicals.

Analysis of the isolated samples showed that passing through Florisil topped with a layer of silica gel did not remove the unreacted thiadiazines **2d** and **2e** but removed the decomposition products and ionic reagents. Pure radicals **1d** and **1e** were obtained in about 10% yield as black crystals by dynamic vacuum sublimation. The solutions of sublimed radical **1e** were green, whereas the sublimed fluorinated radical **1d** formed purple solutions, presumably as a result of the presence of small amounts of impurities.

Crystal and Molecular Structures. Black-purple monoclinic crystals of the fluorinated radical **1d** and black-green triclinic crystals of **1e** were grown by slow gradient sublimation (>100 °C) at 10^{-3} Torr, and their solid structures were determined by X-ray diffraction.[15] All inspected crystals of **1d** and **1e** were twinned. Selected interatomic distances are listed in Table 2, and the molecular structure of **1d** is shown in Figure 2.

Molecules of **1d** are nearly planar, and the largest deviation from planarity of the heterocyclic skeleton of 1.1(6)° is observed for the C(8)−C(9)−C(10)−C(6) angle (Figure 2). The phenyl ring is nearly ideally coplanar with the heterocycle, which results in short H···N nonbonding distances of about 2.44 Å. The solid-state geometry of **1d** is generally well reproduced by the DFT and to lesser degree by HF/6-31G(d) methods. The overall mean difference between 16 experimental and DFT-calculated bond lengths is $\overline{\Delta x} = 0.009$ Å with a STD of 0.013, and $\overline{\Delta x} = 0.006$ Å (STD = 0.011) when the two bonds to sulfur are excluded.

In the solid state, molecules of **1d** are arranged in ideally parallel interpenetrating mirror-imaged stacks rotated by 166° (Figure 3). Within each such column, the S−N bonds overlap, forming an infinite ladder-type structure with the ladder "rungs" slipped by 0.37 Å and an alternating S···N distance of 3.193 and 3.212 Å (Figure 3a). This separation between the ladder "rungs" corresponds to about 93% of the van der Waals separation[16] for the S and N atoms. Each column is related to the neighboring one by an inversion center, and the molecules form weak dimeric pairs with an intermolecular S(1)···N(2) distance of 3.269 Å (or 95% of the sum of the van der Waals radii).[16]

The availability of the crystal structure for thiadiazine **2d**[10] provides an opportunity to examine structural changes upon formation of the radical **1d**. Thus the removal of the 4-H atom from **2d** results in planarization

(14) Masel, R. I. In *Chemical Kinetics and Catalysis*; Wiley&Sons: New York, 2001; pp 97−100.

(15) Crystal data for **1d**: $C_{13}H_5F_4N_2S$ monoclinic, *C*2/*c*, $a = 28.776(11)$ Å, $b = 12.737(5)$ Å, $c = 6.363(3)$ Å, $\beta = 101.095(7)°$, $V = 2288.5(15)$ Å^3, $Z = 8$, $T = 173$ (2) K, $\lambda = 0.71073$ Å, $R(F^2) = 0.0430$ and $R_w(F^2) = 0.1037$ (for 1741 reflections with $I > 2\sigma(I)$). Crystal data for **1e**: $C_{13}H_5Cl_4N_2S$ triclinic, $P\bar{1}$, $a = 6.795(2)$ Å, $b = 8.362(3)$ Å, $c = 13.368(4)$ Å, $\alpha = 71.791(4)°$, $\beta = 83.326(4)°$, $\gamma = 68.631(4)°$, $V = 671.9(4)$ Å^3, $Z = 2$, $T = 173$ (2) K, $\lambda = 0.71073$ Å, $R(F^2) = 0.0847$ and $R_w(F^2) = 0.2067$ (for 1779 reflections with $I > 2\sigma(I)$). For details see Supporting Information.

(16) Rowland, R. S.; Taylor, R. *J. Phys. Chem.* **1996**, *100*, 7384−7391.

TABLE 2. Selected Experimental and Calculated Bond Lengths and Angles for 1d

bond lengths [Å]	exptl	calcd[a]	angles [deg]	exptl	calcd[a]
S(1)−N(2)	1.622(2)	1.656	S(1)−N(2)−C(3)	122.0(2)	122.2
N(2)−C(3)	1.352(4)	1.342	N(2)−C(3)−N(4)	128.7(2)	128.3
C(3)−N(4)	1.320(4)	1.339	C(3)−N(4)−C(5)	120.4(2)	121.3
N(4)−C(5)	1.368(4)	1.360	N(4)−C(5)−C(6)	124.7(3)	125.1
C(5)−C(6)	1.413(4)	1.423	C(5)−C(6)−S(1)	118.9(2)	118.4
S(1)−C(6)	1.733(3)	1.757	C(6)−S(1)−N(2)	105.22(13)	104.8
C(5)−C(7)	1.396(4)	1.418	S(1)−N(2)−C(3)−N(4)	−0.5(6)	0.0
C(6)−C(10)	1.385(4)	1.391	N(2)−C(3)−C(11)−C(16)	0.8(6)	0.0
C(3)−C_{Ph}	1.492(4)	1.489	N(4)−C(5)−C(6)−C(10)	−179.4(4)	180.0

[a] Gas-phase calculations at the B3LYP/6-31G(d) level of theory. The numbering scheme is shown in Figure 2.

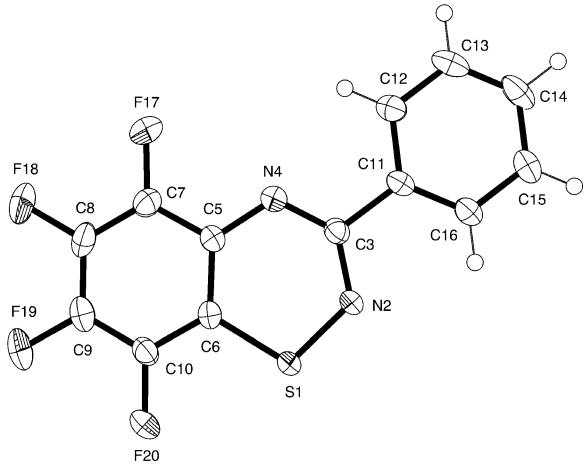

FIGURE 2. Thermal ellipsoids diagram for **1d**. Ellipsoids are drawn at 50% probability and hydrogen atoms have arbitrary radii. Selected molecular dimensions are listed in Table 2.

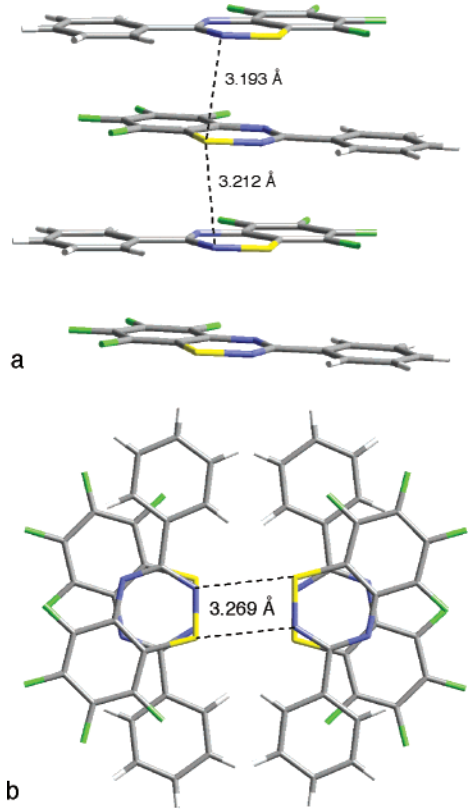

FIGURE 3. Partial packing diagram for **1d** viewed along the tilted *ab* plane (a) and along the *c* axis (b).

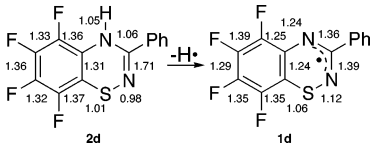

FIGURE 4. Wiberg bond order indices for **2d** and **1d** obtained with the B3LYP/6-31G(d) method.

of the heterocyclic ring due to the change in the number of π electrons from 8 to 7. Also, the removal of the hydrogen makes it possible for the phenyl ring at the C(3) position to adopt a coplanar orientation relative to the heterocycle, and the whole structure becomes planar. The bond lengths in the heterocyclic ring undergo significant changes to reduce bond length alternation. Thus single bonds such as S(1)−N(2) and C(3)−N(4) undergo contraction by nearly 0.06 Å, while the double bond N(2)−C(3) is expanded to about the same extent. Other bonds are adjusted to a lesser extent; most notably the S(1)−C(6) and N(4)−C(5) bonds are contracted, and the C(5)−C(7) bond is expanded by about 0.03 Å. The observed geometrical changes are paralleled by changes in bond orders shown for the **2d**−**1d** pair in Figure 4. This is consistent with aromatization of the heterocycle and the general expectations for the electronic structure of six-membered heterocyclic radicals.[17]

Differences in the molecular geometry and electronic structures between **2d** and **1d** are reflected in the packing diagrams of the two compounds. Arrangement of molecules in the stacks of the 4*H*-thiadiazine **2d** appears to be governed by quadrupolar $\pi-\pi$ interactions between the fluorinated and nonfluorinated benzene rings, as evident from the ∼35% overlap between the rings.[10] In contrast, interactions between the thiadiazine rings appear to be the dominant factor in molecular packing of radical **1d**. This is evident from the nearly ideal antiparallel arrangements of the N−S bonds and generally good overlap of the thiadiazine rings but not the benzene rings (Figure 3b).

The crystals of the tetrachloro radical **1e** were generally of less than desirable quality and were plagued with twinning. Three crystals were analyzed using either conventional X-ray or synchrotron radiation, but none of them gave data that would permit the structure solution and refinement to *R* smaller than 8.5%. The X-ray diffraction results indicate that the molecular structure of **1e** is as expected from theoretical predictions and

(17) Oakley, R. T. *Prog. Inorg. Chem.* **1988**, *36*, 299−391.

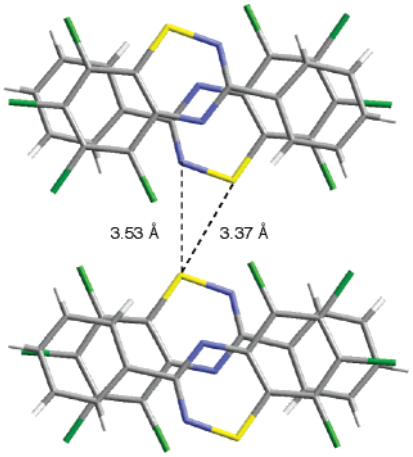

FIGURE 5. Partial packing diagram for **1e** viewed along the tilted *a* axis.

similar to that of **1d** (Figure 2). The relatively large error on the molecular dimensions does not allow for a detailed comparison of **1e** on the molecular level. The data provide, however, useful information about crystal packing in **1e**, which can be compared with that of **1d**.

Molecules of **1e** are, like **1d**, arranged in antiparallel interpenetrating stacks along the *a* axis. The arrangement maximizes the overlap between benzene rings at the expense of the overlap between the thiadiazinyls (Figure 5). Unlike in the crystal structure of **1d**, molecules of **1e** in each stack are related to molecules in the other stack and also in the neighboring column by an inversion center. The intermolecular separation within a column is about 3.40 Å, which is about 0.25 Å greater than in **1d**. The S···S nonbonding distance for molecules in neighboring columns is about 3.37 Å, which corresponds to 94% of the sum of the van der Waals radii.[16]

Computational results show that other radicals **1a**−**1c** are also planar with C_s molecular symmetry. The interatomic distances and angles of the thiadiazine ring remain practically the same throughout the series with a typical variation in the bond length of about 0.03 Å. Most noticeably, the N(4)−C(5) distance varies from 1.358 Å for **1c** and **1e** to 1.369 Å for **1a**. This presumably reflects the π interactions between the nitrogen atom and the other fused ring. For the relatively electron-rich benzo derivative **1a** the distance is longest, whereas for the electron-deficient tetrachloro and pyrazino derivatives **1c** and **1e** the distance is shortest. The analogous S(1)−C distance is less sensitive to electronic effects in the fused ring.

ESR Spectroscopy. Room-temperature solution spectra of radicals **1c** and **1e** exhibit five unresolved signals arising from coupling to the thiadiazinyl nitrogen atoms (Figure 6). In the benzo and pyrido derivatives **1a** and **1b**, each line of the quintet is split by interactions with H atoms. The spectrum of **1d** is significantly more complicated as a result of additional coupling with fluorine atoms. All spectra are centered at about 3475 G.

All spectra except for **1b** were numerically simulated using initial hyperfine coupling constant (hfcc) values obtained from B3LYP/cc-pVDZ//B3LYP/6-31G(d) calculations and appropriately scaled.[18] After a least-squares fit for nine parameters (including all hydrogen atoms of the

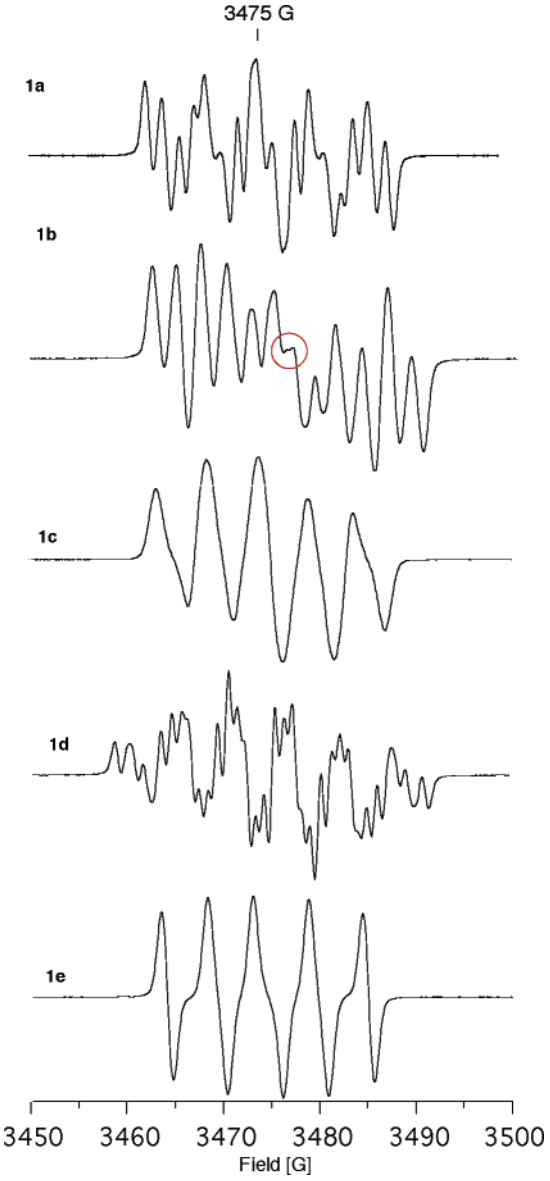

FIGURE 6. ESR spectra for **1** recorded in benzene at ambient temperature. Solutions of **1a**−**1c** were generated using Method B, and solutions of **1d** and **1e** were obtained from sublimed samples. The circle indicates the symmetry anomaly.

phenyl substituent), the correlation factors r were >0.99 for all pairs of simulated and experimental spectra except for **1d** (r = 0.973). The resulting hfcc values were assigned to the molecular structures on the basis of trends in the calculated values and are listed in Table 3.

Spectra of the pyrido radical **1b** consistently lacked symmetry in the central part (Figure 6), and none of them could be simulated. Therefore, the spectrum of **1b** was reflected about the midpoint defined by the pairs of spectral peaks and assumed to be lying in the middle of a small central peak (cf. spectrum of **1a**). The transformed spectrum of **1b** was simulated (r = 1.00), and the hfcc values are listed in Table 3.

All five radicals show two similar couplings of about 6 and 5 G to the thiadiazinyl nitrogen atoms N(2) and N(4), which results in the basic quintet in the spectrum.

(18) Kaszynski, P. *J. Phys. Chem. A*, **2001**, *105*, 7615−7625.

TABLE 3. Experimental Isotropic hfcc [G] for Radicals 1

	radical				
	1a	**1b**	**1c**	**1d**	**1e**
g	2.0056	2.0055	2.0058	2.0056	2.0057
a_{N2}	5.92	5.96	5.57	5.92	5.74
a_{N4}	4.86	4.94	4.49	5.38	4.71
a_{X5}[b]	1.31	1.85	0.62	2.02	0.09
a_{X6}[b]	0.02	0.06	0.07	1.04	0.00
a_{X7}[b]	2.06	2.60	1.82	4.68	0.26
a_{X8}[b]	0.32	0.53	0.29	1.65	0.16
$a_{H(Ph)}$ ortho	0.47	0.43	0.36	0.31	0.35
$a_{H(Ph)}$ meta	0.20	0.23	0.17	0.20	0.18
$a_{H(Ph)}$ para	0.37	0.36	0.24	0.3	0.25

[a] Obtained from simulation of the experimental spectra to the correlation value $r > 0.99$ ($r = 0.973$ for **1d**). [b] X is H, N, F (**1d**), or Cl (**1e**).

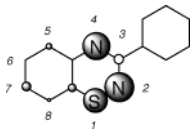

FIGURE 7. Total spin distribution in **1a** calculated with the B3LYP/cc-DVZ//B3LYP/6-31G(d) method. The numerals show the heterocycle numbering system.

Additional splitting in the spectrum results from coupling to atoms in positions 5 and 7, and in the case of **1d** also to F in position 8 ($a_{F8} = 1.65$ G). The remaining hfcc are small, typically <0.4 G, and they contribute to line broadening. This is consistent with the spin distribution in the heterocyclic ring shown for **1a** in Figure 7.

The spectrum of the pyrazino derivative **1c** recorded under various conditions consistently shows no fine structure of the five broad lines despite the expected relatively high a_{N5} and a_{H7} values. This can be attiributed to the low yield of the radical (<4%) and high concentration of the unreacted precursor **2c** (> 90%) in the crude solution, and possible interactions between **1c** and **2c**. These interactions may also affect the hfcc values, which significantly deviate from those theoretically predicted. This is consistent with a similar observation for **1a**; solutions of crude **1a** generated using Method A and containing >50% of unreacted **2a** show only five unresolved lines, whereas a nicely resolved spectrum of **1a** (Figure 6) was obtained for crude solutions generated using Method C and containing mostly radical **1a**.

The hfcc's obtained from simulations of experimental spectra generally correlate well with the calculated values. The only significant exceptions are the a_H values for **1c** and the overestimated a_F value assigned to F(6). The scaling factor resulting from the best fit line for a_H values is very similar to that established earlier,[18] but for a_N the factor is slightly smaller (0.73 vs 0.767).[18] This is due to systematic overestimation of the hfcc values by about 0.4 G for the N(4) atom in all radicals **1**. Nevertheless, overall good agreement with the previous scaling factor and high correlation values ($R^2 = 0.99$) demonstrate the validity of our protocol for prediction of hfcc in this class of radicals.[18] The calculated hfcc for the chlorines are overestimated by a factor 1.86 ($R^2 = 0.97$).

All g values measured for the radicals are about 2.006 (Table 3), which reflect very similar and relatively large spin concentrations on the sulfur atoms (0.28; see Figure 7).

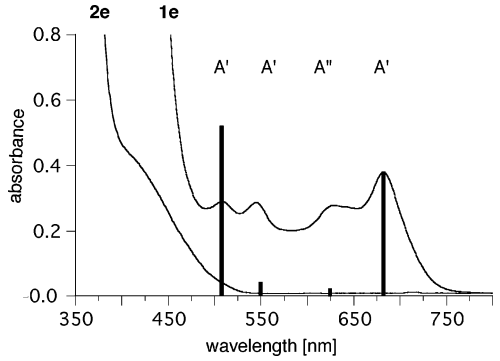

FIGURE 8. Absorption spectra of **2e** ($c \approx 10^{-4}$ M) and **1e** ($c \approx 10^{-3}$ M) recorded in toluene. Vertical bars represent calculated absorption bands with indicated symmetry and scaled by $E_{exp} = 0.97E_{calcd} - 0.12$ [eV]. The height represents relative oscillator strength.

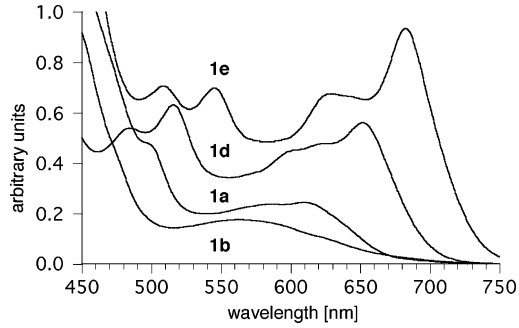

FIGURE 9. Low energy portion of the absorption spectra for selected radicals recorded in toluene. Sublimed **1d** and **1e** and crude solutions of **1a** and **1b** were used. The vertical scale is arbitrary and does not reflect the relative absorption coefficients.

Electronic Absorption Spectroscopy. Oxidation of thiadiazines **2** to radicals **1** results in the appearance of new low energy and low intensity absorption bands above 500 nm. This is demonstrated for **1e** in Figure 8 and compared for four radicals in Figure 9. The halogenated radicals **1d** and **1e** show four maxima above 450 nm (Table 4). In the benzo derivative **1a** only three such maxima could be distinguished, while the pyrido derivative **1b** has one broad featureless absorption band with the maximum at 563 nm. Their longest wavelength absorption bands range from 682 nm for the tetrachloro radical **1e** to 611 nm for the benzo derivative **1a**. This order is well reproduced by TD-DFT calculations, which also show that the lowest energy band of the pyrido derivative **1b** should be about that for **1e** (682 nm). The analogous excitation energy for the pyrazino radical **1c** is predicted to be lowest in the series (Table 4).

A comparison of 11 experimental excitation energies clearly identified for **1a**, **1d**, and **1e** with those calculated in a vacuum at the B3LYP/6-31G(d) level of theory shows an excellent correlation (Figure 10). All computed energies are systematically overestimated by 0.17 eV. The appropriately scaled theoretical excitation energies for **1e** are shown in Figure 8 with sizes indicating relative oscillator strength. The energies, calculated using diffuse functions on heavy atoms (B3LYP/6-31+G(d)//B3LYP/6-

TABLE 4. Experimental[a] and Calculated[b] Lowest Energy Electronic Absorption Bands for Radicals 1

a [nm]		**b** [nm]		**c** [nm]		**d** [nm]		**e** [nm]	
exptl	calcd	exptl[c]	calcd	exptl[d]	calcd	exptl	calcd	exptl	calcd
609.7	561.7 (11) A′		631.9 (1) A″		702.3 (0.3) A″	651.7	608.3 (15) A′	682.4	624.8 (19) A′
585.7	556.3 (1) A″		558.1 (12) A′		587.0 (15) A′	603.0	544.5 (1) A″	628.9	573.3 (1) A″
505.7	477.7 (4) A′		468.4 (5) A′		473.3 (3) A′	515.7	488.4 (2) A′	545.2	508.6 (2) A′
	417.2 (20) A′		432.4 (7) A′		467.2 (6) A′	484.2	453.0 (9) A′	508.5	469.8 (26) A′

[a] Obtained in toluene solution. [b] TD-B3LYP/6-31G(d); in parentheses oscillator strength $\times 10^3$. [c] One broad absorption band with a maximum at 563 nm. [d] Not studied experimentally.

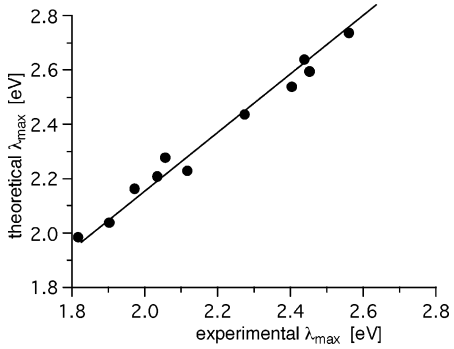

FIGURE 10. Experimental (recorded in toluene) versus theoretical (TD-B3LYP/6-31G(d)) low energy absorption bands for **1a**, **1d**, and **1e**. The best fit line: $E_{calcd} = 1.00E_{exp} + 0.17$ ($R^2 = 0.984$).

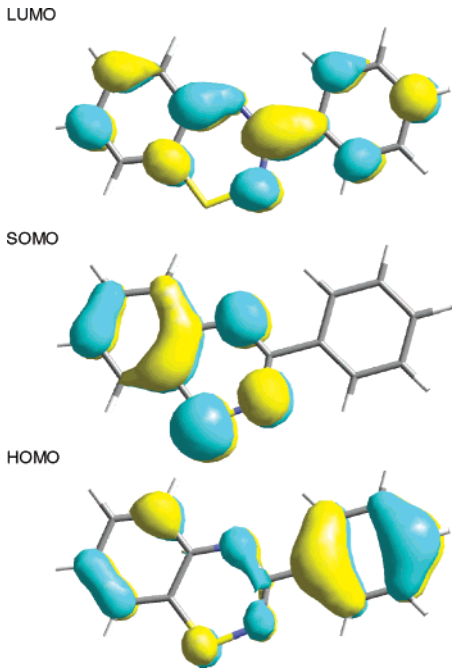

FIGURE 11. HOMO, SOMO, and LUMO contours for **1a** (B3LYP/6-31G(d,p))

31G(d)), are overestimated by about 0.3 eV and with a lower correlation factor ($R^2 = 0.972$).

Computational analysis shows that the several lowest energy transitions in radicals **1** involve the HOMO, SOMO, and LUMO orbitals shown in Figure 11 for **1a**. For instance, the lowest energy excitations for the benzo and tetrahalobenzo derivatives **1a**, **1d**, and **1e** involve largely the HOMO−SOMO transition with a smaller, about 30%, component of the SOMO−LUMO transition. The next lowest energy absorption band originates from the pure HOMO-2 to SOMO transition for **1a** or HOMO-3 to SOMO transition for **1d** and **1e**. All orbitals involved in these transitions are of π symmetry except for the HOMO-2 for **1a**, which includes the lone electron pairs of the thiadiazine ring.

The lowest energy excitations in the pyrido and pyrazino derivatives **1b** and **1c** result largely from the HOMO-1−SOMO transitions. In these two radicals the HOMO-1 includes the thiadiazine ring lone pairs. The next two lowest energy excitations in **1c** appear to be analogous to the two longest wavelength excitations in the benzo derivative **1a**. The HOMO−SOMO and SOMO−LUMO transitions are the main components of the second and third lowest energy absorption bands for **1b**, respectively.

All five radicals have the electronic state ^{2}A″ and the unpaired electron resides on the π MO (−5.44 eV for **1a**, −5.65 eV for **1b**, −5.94 eV for **1c**, −6.04 eV for **1d**, and −5.94 eV for **1e**, according to the B3LYP/6-31+G(d)//B3LYP/6-31G(d) method).

Chemical Stability of Radicals. Generation of and attempts to isolate radicals demonstrated that their stability increases in the order **1a** < **1b** < **1d** ≈ **1e**. All radicals appear to be stable in cold toluene solutions (−80 °C). Upon warming and exposure to air the green color of the radicals bleaches, forming colorless solutions. The only exception is the fluorinated radical **1d**, for which one of the minor decomposition products is purple with a single maximum of absorption at 558 nm. This unidentified product is formed in trace quantities during sublimation of **1d** and gives a pink color to the solution of the sublimed material. Its presumed presence, however, was not clearly confirmed by UV−vis spectroscopy (see Figure 9) or during solution of crystal structure (vide supra).

The main decomposition products of radicals **1** in air appear to be the corresponding *S*-oxides **4**, which were isolated and characterized for **1a** and **1e**. The nonvolatile **4e** was also isolated in about 70% yield from a residue after sublimation of radical **1e**.

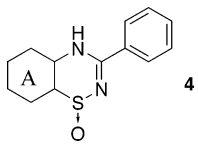

4

Quantitative ESR studies of stability were conducted in benzene at ambient temperature using sublimed halogenated radicals **1d** and **1e**, and solutions of **1a**−**1c** generated with AgO/K_2CO_3 (Method B). Analysis of the kinetic data (Figure 12) shows that the stability of the radicals follows the order **1c** < **1a** < **1b** < **1e** < **1d**, which is largely consistent with our qualitative observations

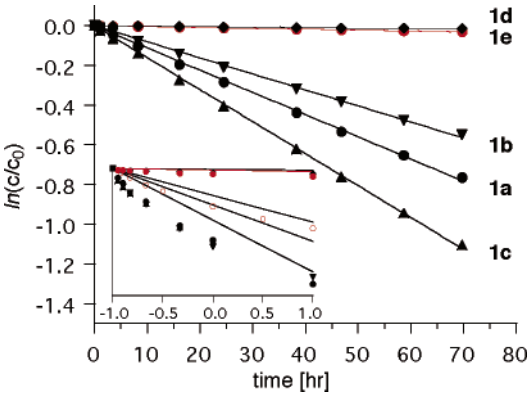

FIGURE 12. Intensity of ESR signal for radicals **1** as a function of time recorder at abmbient temerature. Solutions of crude **1a**−**1c** and sublimed **1d** and **1e** in benzene were degassed and filled with Ar. Open circle datapoints were obtained for a sample of **1e** kept under vacuum. Rate of decomposition: **1a**, $k = 112 \times 10^{-4}$ h^{-1}; **1b**, $k = 81 \times 10^{-4}$ h^{-1}; **1c**, $k = 161 \times 10^{-4}$ h^{-1}; **1d**, $k = 2.3 \times 10^{-4}$ h^{-1}; **1e**, $k = 4.4 \times 10^{-4}$ h^{-1}. Correlation coefficients $R^2 \geq 0.994$. The inset shows the initial 2 h of the measurement.

(vide supra). The most stable fluorinated radical **1d** decomposes over 60 times more slowly than the least stable pyrazino derivative **1c** and has a half-life in solution of over 4 months. The stabilities of the unisolated **1a**−**1c** probably represent the lower limit, based on the results for **1e** (vide infra).

The kinetic analysis was performed on data acquired 1 h after the radical preparation to allow the radicals to consume any residual oxygen. During the initial hour the plots are nonlinear, as shown in the inset in Figure 12. Samples prepared in the same manner but kept under vacuum rather than Ar slowly leaked air, and the nonlinear behavior persisted for many hours, especially for **1a**−**1c**.

In another set of experiments, the stability of degassed benzene solution of sublimed **1e** was investigated using UV−vis spectroscopy by monitoring the intensity of absorption at 680 nm. During the first 5 h the kinetics of radical decay appeared to be pseudo-zero-order with a rate constant $k = 1.2 \times 10^{-4}$ s^{-1}, which suggests photochemical instability of the radical. A similar analysis for the crude unsublimed solid **1e** showed about 10 times faster decomposition of the radical. In contrast, a degassed and subsequently aerated (15 s) solution of **1e** showed rapid decomposition during the initial 2 h, which can be described as pseudo-first-order with a rate constant $k \approx 1.1$ h^{-1}.

The stability of **1e** toward other reagents was briefly investigated. Addition of about 10 equiv of EtOH, Et_3N, or AcOH to a toluene solution of **1e** had little effect on the decay of the absorption band at 680 nm, and the rate was approximately the same as that when the sample was exposed to air. In the case of EtOH and AcOH, the main product of decomposition was identified as **4e**, whereas in Et_3N generation of large amounts of starting thiadiazine **2e** was observed on the basis of TLC analysis.

Cyclic Voltammetry. Electrochemical analysis of the two halogenated radicals **1d** and **1e** showed strongly irreversible oxidation behavior with the cathodic potential peak at 1.2 V and a reversible reduction at about 0

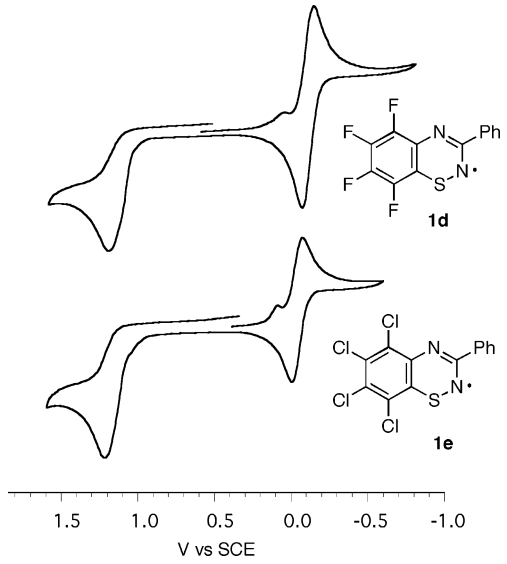

FIGURE 13. CV scan of **1d** (top) and **1e** (bottom) in CH_2Cl_2, [n-Bu_4N][PF_6] supporting electrolyte and 0.10 V/min scanning rate.

TABLE 5. Solution Half-Wave[a] and Cell Potentials for Radicals 1d and 1e

	$E_{1/2}^{red}$[b] [V]		$E_{1/2}^{ox}$[c] [V]		E_{cell}[d] [V]	
radical	CH_2Cl_2	MeCN	CH_2Cl_2	MeCN	CH_2Cl_2	MeCN
1d	−0.11[e]	−0.17	+1.20	+1.03	+1.26	+1.20
1e	−0.04[f]	*g*	+1.20	*g*	+1.20	*g*

[a] Referenced to ferrocene set at +0.38 V in MeCN and +0.48 V in CH_2Cl_2. [b] Quasireversible behavior. [c] Irreversible behavior; E_{pc} value listed. [d] E_{cell} estimated as $E_{pc1/2}^{ox} - E_{pc1/2}^{red}$. [e] Pre-peak at +0.04 V. [f] Pre-peak at +0.08 V. [g] Insufficient solubility.

V. Typical electrochemical waves for **1d** and **1e** are shown in Figure 13, and half-wave potentials are listed in Table 5. The tetrafluoro radical **1d** was analyzed in MeCN and CH_2Cl_2, whereas the tetrachloro **1e** was studied only in CH_2Cl_2 because of its poor solubility in MeCN.

Cyclic voltammetry of the radicals shows pre-peaks, which are 0.15 V (for **1d**) and 0.12 V (for **1e**) more positive than the appropriate anodic peaks. The pre-peak current decreases proportionally to the increase of the scan rate, which suggests surface adsorption of the reduced species. Such behavior was observed before for other heterocyclic radicals.[19] The observed lower reduction potential for **1d** in MeCN than in CH_2Cl_2 is consistent with other experimental data.[20]

The experimental redox potentials for **1d** and **1e** are consistent with values estimated from the calculated and appropriately scaled ionization potentials I_p, electron affinities EA, and disproportionation energies in Table 6. Thus, the previously established correlations[21] predict a reduction potential of −0.05 V for **1d** and a +0.06 V difference in $E_{1/2}^{red}$ between **1e** and **1d** in MeCN, while the experimental values are −0.17 V and +0.07 V, respectively. Also the estimated and experimental oxida-

(19) Boeré, R. T.; Moock, K. H.; Parvez, M. *Z. Anorg. Allg. Chem.* **1994**, *620*, 1589−1598.
(20) Boeré, R. T.; Roemmele, T. L. *Coord. Chem. Rev.* **2000**, *210*, 369−445.
(21) Kaszynski, P. *J. Phys. Chem. A* **2001**, *105*, 7626−7633.

TABLE 6. Calculated[a] Parameters for Radicals 1

	radical				
	1a	**1b**	**1c**	**1d**	**1e**
I_p (vert)[b] [eV]	6.80	7.03	7.30	7.26	7.17
EA[c] [eV]	1.98	2.16	2.48	2.58	2.66
$E_{1/2}^{red}$[d] [V]	−0.50	−0.37	−0.13	−0.05	+0.01
ΔE_{SCF}^{1}[e] [kcal/mol]	123.2	123.4	122.6	123.2	114.6
ΔE_{SCF}^{2}[f] [kcal/mol]	−8.0	−6.9	−7.4	−8.9	−7.7
$\Sigma\Delta E_{SCF}$[g] [kcal/mol]	115.2	116.5	115.3	114.3	107.0
$\Sigma\Delta G_{298}$[h] [eV]	5.04	5.04	5.01	4.98	4.63
E_{cell}[i] [V]	1.1	1.1	1.1	1.0	1.0
$E_{1/2}^{ox}$[j] [V]	+0.6	+0.7	+0.9	+1.0	+1.0

[a] B3LYP/6-31G(d) level of theory for I_p and B3LYP/6-31+G(d)//B3LYP/6-31G(d) for all others. Calculated values are scaled using factors in ref 21. [b] Difference in SCF energies. [c] Difference in ZPE-corrected SCF values. [d] Reduction potential in MeCN obtained from computed EA; ref 21. [e] Electron-transfer energy between two radicals to form an ion pair. [f] Reorganization energy to form a relaxed ion pair. [g] Total SCF energy for radical disproportionation. [h] Total free energy of radical disproportionation. [i] Electrochemical cell potential calculated from $\Sigma\Delta E_{SCF}$. [j] Oxidation potentials in MeCN calculated from $E_{1/2}^{ox} = E_{cell} + E_{1/2}^{red}$.

tion potentials $E_{1/2}^{ox}$ for **1d** in MeCN are essentially the same and about +1.0 V. The electrochemical window for **1d** in MeCN is predicted to be bigger by about 0.2 V than found experimentally, but considering the uncertainty of the prediction[21] and the irreversibility of the oxidation process, the comparison is rather good.

A comparison of the series of five radicals **1a**−**1e** in Table 6 shows trends expected on the basis of the electronic properties of the ring fused to the thiadiazine. The most electron-rich benzothiadiazinyl **1a** has the lowest estimated ionization and oxidation potentials (6.80 eV and +0.6 V respectively). At the same time, **1a** also has the lowest EA and reduction potential in the series. On the other hand, the tetrachloro **1e**, closely followed by tetetrafluoro derivative **1d**, has the highest estimated reduction and oxidation potentials and EA in the series. The pyrazino derivative **1c** has the highest value of I_p = 7.30 eV, which is higher by 0.50 eV than that for the benzo derivative **1a**. The estimated E_{cell} for all five radicals is similar and just above 1 V, while the electrochemical window moves from $E_{1/2}^{red} = -0.5$ V for most electron-rich system **1a** toward positive values reaching the estimated $E_{1/2}^{red} = 0.0$ V for **1e**.

The calculations show that radicals **1** have relatively small disproportionation energies of about 122 kcal/mol (about 5 eV). The exception in the series is the tetrachloro derivative **1e**, which has the lowest energy change upon the formation of an ion pair. The value of 114.6 kcal/mol is comparable with that calculated for phenalenyl radical,[21] but all ions derived from radicals **1** still have a significant reorganization energy of about 7−9 kcal/mol. The lowest reorganization energies are found for ions derived from three radicals **1b**, **1c**, and **1e**, which maintain the C_s molecular symmetry. The anions derived from **1a** and **1d** are significantly puckered and also have the highest reorganization energies of −8.0 and −8.9 kcal/mol, respectively.

Discussion

Method A (PbO_2) is the most common way to generate thioaminyl radicals from the corresponding N−H compounds, but only modest yields have been observed.[5,8,22] The addition of MeCN to the reaction mixture significantly increases the yield of the radicals and works particularly well with AgO, a more potent oxidant (Method C). This effect of MeCN cosolvent on the rate of electron transfer from the substrate to the metal oxide is presumably due to (i) increased polarity of the medium, (ii) more complete deprotonation of the substrate, (iii) coordination of the solvent to silver ions, or (iv) a combination of the above. Experiments show that the presence of a base and high dielectric medium is important for fast rate and complete generation of radicals. Unfortunately, the use of a polar aprotic solvent also makes the base more reactive, which appears to have a detrimental effect on the pyrido and pyrazino derivatives **1b** and **1c**. It is possible that this method will find more general use in preparation of other radicals.

The observed trend in stability of the five radicals established in Figure 12, **1c** < **1a** < **1b** ≪ **1e** < **1d**, generally is consistent with expectations, except for pyrazino derivative **1c**. Thus, incorporation of an N atom into the benzene ring of **1a** to form the pyrido derivative **1b** increases the radical's stability by a factor of 1.4. However, contrary to expectations, the pyrazino derivative with one more N atom is less stable than the benzo analogue **1a** by the same factor. It would be interesting to compare the stability of **1b** to that of its isomer, which could be generated from the known 4*H*-pyrido[2,3-*e*]-[1,2,4]thiadiazine.[23]

The significant stability of the tetrachloro derivative **1e** was expected on the basis of ample literature examples.[24] In contrast, π radicals fluorinated at the high spin density sites are rare,[25] and to our knowledge no comparative studies of stability of the chlorinated and fluorinated radicals have been performed. Our studies demonstrate that fluorine atoms may be even more effective substituents than chlorine in stabilization of π delocalized radicals. This finding is advantageous for the design of liquid crystals,[7] since the smaller fluorine atoms are much preferred to the larger chlorines.

The chemical stability of the halogenated radicals is sufficient for further studies of liquid crystalline derivatives of **1d** and also **1e**. Both radicals can be chromatographed, and they show low sensitivity to protic solvents but suffer from sensitivity to oxygen. Thus future work and characterization of radical derivatives will require an anaerobic atmosphere. The reaction of **1** with oxygen takes place at the sulfur center and gives rise to the *S*-oxides **4**. Fortunately, the resulting *S*-oxides can, in principle, be reduced to 4*H*-thiadiazines **2** with phosphines.[26]

Although our main focus is on liquid crystalline derivatives of **1**, we have also briefly considered the suitability of **1** for molecular conductors. Our computational results

(22) For example: Miura, Y.; Oyama, Y.; Teki, Y. *J. Org. Chem.* **2003**, *68*, 1225−1234.
(23) Gilchrist, T. L.; Rees, C. W.; Vaughan, D. *J. Chem. Soc., Perkin Trans. 1* **1983**, 55−59.
(24) Ballester, M. *Adv. Phys. Org. Chem.* **1989**, *25*, 267−446 and references therein.
(25) Höfs, H.-U.; Bats, J. W.; Gleiter, R.; Hartmann, G.; Mews, R.; Eckert-Maksic, M.; Oberhammer, H.; Sheldrick, G. M. *Chem. Ber.* **1985**, *118*, 3781−3804.
(26) Finch, N.; Ricca, S., Jr.; Werner, L. H.; Rodebaugh, R. *J. Org. Chem.* **1980**, *45*, 3416−3421.

in Table 6, supported by voltammetric studies, indicate that the redox properties of the radicals are generally favorable in the context of molecular conductors.[28] Radicals **1** appear to have a relatively small, about 1.1 V, electrochemical window, whose position can be tuned within at least 0.5 V. The values of E_{cell} for **1** and also the disproprtionation energies of about 122 kcal/mol compare favorably to 4-aryl-[1,2,3,5]dithiadiazolyls[18,29] but are still significantly larger than those for recently reported radicals.[30] Particularly interesting in this context is the tetrachloro radical **1e**, which has the lowest disproportionation energy in the series and a relatively small expected electron−phonon coupling since both ions preserve the C_s symmetry of the radical. It is likely, however, that the redox properties of **1** and hence on-site Coulomb repulsion can be optimized further. For instance, placing the phenyl group at the 3 position significantly lowered both values in the parent benzo-[1,2,4]thiadiazinyl. [21]

Experimental and theoretical results indicate a planar geometry of the radicals, which combined with their packing properties may be of interest for the design of semiconductive solids. The crystal structure of **1d** has a rare, ladder-type infinite chain of almost evenly spaced S−N rungs (Figure 3). A similar columnar arrangement of the heterocycles is often found in dithiadiazolyls,[27] but unlike in **1d**, the stacks are composed of dimeric pairs with large alternations of the S···N (and S···S) distances (Peierls-type distortion). This packing of **1d** in columns appears to be driven by the SOMO−SOMO overlap and overall results in diamagnetic solids. This is evident from the less than 1% of spin concentration found by ESR in sublimed **1d** at ambient temperature. Materials with such low spin concentrations are not expected to exhibit high electron conduction.

The crystal packing of **1e** is distinctly different from that of **1d**. The larger size of chlorine atoms does not allow for efficient SOMO−SOMO interactions within a column, and molecules form dimeric pairs through in-plane weak S···S interactions. The crystallographic results for **1d** and **1e** suggest rich opportunities for the engineering of solid-state structures and hence properties of substituted benzo[1,2,4]thiadiazinyls. A variety of such structures can, in principle, be obtained easily through a recently described method.[10]

Conclusions

Among the five investigated fused-ring [1,2,4]thiadiazinyl radicals only the halogenated derivatives **1d** and **1e** can be generated conveniently in high yields, isolated chromatographically, and purified by vacuum sublimation. The two radicals are practically inert to atmospheric oxygen in the solid state, but their solutions decompose quickly in air. This indicates that both of the halogenated radicals are suitable as structural elements for liquid crystalline compounds. Such materials should be sufficiently stable for future investigation, if air is rigorously excluded. In this context, 4*H*-thiadiazine **2d**, a precursor to the apparently most stable fluorinated radical **1d**, was appropriately substituted with liquid-crystallinity-promoting groups, and the corresponding radicals are being studied.[31]

Computational Details

Quantum-mechanical calculations were carried out at the B3LYP/6-31G(d) level of theory[32,33] using the Linda-Gaussian 98 package[34] on a Beowulf cluster of 16 processors. Geometry optimizations were undertaken using appropriate symmetry constraints and tight convergence limits. Vibrational frequencies were used to characterize the nature of the stationary points and to obtain thermodynamic parameters. Zero-point energy (ZPE) corrections were scaled by 0.9806.[35] The Wiberg bond order indices were obtained using the NBO algorithm[36] supplied in the Gaussian package.

The Fermi constants were calculated at the B3LYP/cc-pVDZ//B3LYP/6-31G(d) and converted to hfcc's. The a_{Cl} values for the natural isotopic abundance of $^{35/37}$Cl were obtained using a conversion factor of 420.183.

Electronic excitation energies for the radicals were obtained at the B3LYP/6-31G(d) level using the time-dependent DFT calculations[37] supplied in the Gaussian package. Following general recommendations,[38] energy changes and differences were derived as the differences of SCF energies of individual species computed using the diffuse function-augmented 6-31+G(d) basis set at the geometries obtained with the 6-31G(d) basis set (single point calculations). Thermodynamic corrections were obtained using the 6-31G(d) basis set.

Experimental Section

X-band ESR spectra were obtained using modulation amplitude 0.10 G and spectral width of 100 G. Solutions in distilled benzene were degassed by three freeze/pump/thaw cycles. Spin concentration and yields were calculated by double integration of the ESR signal of the sample and of a measured amount of 4-hydroxy-TEMPO radical purchased from Aldrich and assumed to be 100% pure. Samples were referenced using strong pitch with $g = 2.0028$. PbO_2 and K_2CO_3 were dried in a vacuum at 100 °C for 24 h, in the presence of P_2O_5. AgO

(27) For example: Banister, A. J.; Hansford, M. I.; Huptman, Z. V.; Wait, S. T.; Clegg, W. *J. Chem. Soc., Dalton Trans.* **1989**, 1705−1713. Bricklebank, N.; Hargreaves, S.; Spey, S. E. *Polyhedron* **2000**, *19*, 1163−1166. Bond, A. D.; Haynes, D. A.; Pask, C. M.; Rawson, J. M. *J. Chem. Soc., Dalton Trans.* **2002**, 2522−2531.

(28) Garito, A. F.; Heeger, A. J. *Acc. Chem. Res.* **1974**, *7*, 232−240. Haddon, R. C. *Aust. J. Chem.* **1975**, *28*, 2343−2351. Torrance, J. B. *Acc. Chem. Res.* **1979**, *12*, 79−86.

(29) Boeré, R. T.; Moock, K. H. *J. Am. Chem. Soc.* **1995**, *117*, 4755−4760.

(30) Beer, L.; Brusso, J. L.; Cordes, A. W.; Godde, E.; Haddon, R. C.; Itkis, M. E.; Oakley, R. T.; Reed, R. W. *Chem. Commun.* **2002**, 2562−2563.

(31) Fryszkowska, A.; Zienkiewicz, J.; Sienkowska, M.; Kaszynski, P. Unpublished results.

(32) Becke, A. D. *J. Chem. Phys.* **1993**, *98*, 5648−5652.

(33) Lee, C.; Yang, W.; Parr, R. G. *Phys. Rev. B* **1988**, *37*, 785−789.

(34) *Gaussian 98*, Revision A.9; Frisch, M. J.; Trucks, G. W.; Schlegel, H. B.; Scuseria, G. E.; Robb, M. A.; Cheeseman, J. R.; Zakrzewski, V. G.; Montgomery, J. A. Jr.; Stratmann, R. E.; Burant, J. C.; Dapprich, S.; Millam, J. M.; Daniels, A. D.; Kudin, K. N.; Strain, M. C.; Farkas, O.; Tomasi, J.; Barone, V.; Cossi, M.; Cammi, R.; Mennucci, B.; Pomelli, C.; Adamo, C.; Clifford, S.; Ochterski, J.; Petersson, G. A.; Ayala, P. Y.; Cui, Q.; Morokuma, K.; Malick, D. K.; Rabuck, A. D.; Raghavachari, K.; Foresman, J. B.; Cioslowski, J.; Ortiz, J. V.; Baboul, A. G.; Stefanov, B. B.; Liu, G.; Liashenko, A.; Piskorz, P.; Komaromi, I.; Gomperts, R.; Martin, R. L.; Fox, D. J.; Keith, T.; Al-Laham, M. A.; Peng, C. Y.; Nanayakkara, A.; Challacombe, M.; Gill, P. M. W.; Johnson, B.; Chen, W.; Wong, M. W.; Andres, J. L.; Gonzalez, C.; Head-Gordon, M.; Replogle, E. S.; Pople, J. A. Gaussian, Inc.: Pittsburgh, PA, 1998.

(35) Scott, A. P.; Radom, L. *J. Phys. Chem.* **1996**, *100*, 16502−16513.

(36) Glendening, E. D.; Reed, A. E.; Carpenter, J. E.; Weinhold, F. *NBO*, version 3.1.

(37) Casida, M. E.; Jamorski, C.; Casida, K. C.; Salahub, D. R. *J. Chem. Phys.* **1998**, *108*, 4439−4449.

(38) Clark, T.; Chandrasekhar, J.; Spitznagel, G. W.; Schleyer, P. v. R. *J. Comput. Chem.* **1983**, *4*, 294−301.

was prepared according to a literature procedure[39] and dried as above at 50 °C.

Simulation of the ESR spectra was done with the PEST program (version 0.96 for Windows; available at http//epr.niehs.nih.gov/pest.html) using the scaled[18] DFT results for the input. The resulting hfcc's were perturbed until the global minimum for the fit was achieved. Spectra used for simulation were generated by reflection of the left half of each spectrum. Major absorption bands in IR spectra were assigned on the basis of general trends and comparison with the results of DFT calculations.

Electronic Absorption Spectra. Spectra of **1d** and **1e** were recorded for solution of solid radicals in dry toluene at ambient temperature. About 1 mM solutions of **1a** and **1b** were generated in dry toluene with AgO/K_2CO_3, filtered through a microfilter, and transferred to a UV cell.

Generation of Radicals. Methods A and B. Precursor **2** (0.01 mmol) was dissolved in degassed dry benzene (10 mL, 1 mM solution) and stirred over well-ground PbO_2 (24 mg, 0.10 mmol, Method A) or AgO (12.5 mg, 0.10 mmol, Method B) and K_2CO_3 (14 mg, 0.10 mmol) for 15 min under an atmosphere of dry N_2. The solution acquired a dark green color. To monitor progress of the reaction, several samples, the first 5 min after the beginning of the experiment, were taken from the reaction mixture, and the amount of the radical was quantified by ESR spectroscopy. Typically, a 0.5-mL sample was transferred to an ESR tube using a syringe and a microfilter and carefully degassed before taking the measurement.

Method C. Similar to Method B except for using a 1:1 mixture of MeCN and toluene as the solvent. Samples of the solution were taken initially every 15 s to record the absorbance at 610 nm for **1a**, and 680 nm for **1e**.

On a 10 mmol preparative scale, **1d** and **1e** were obtained by oxidation of **2d** and **2e** respectively, with AgO/K_2CO_3 at ambient temperature. After vigorously stirring for 90 s, the resulting black-green reaction mixture was diluted with toluene and filtered through a short jacketed column (5 cm of Florisil topped with 0.5 cm of silica) below 0 °C. Solvents were removed under reduced pressure (~1 Torr) at temperatures below 0 °C, leaving a black-green solid of **1**. Radicals **1d** and **1e** were sublimed in a vacuum (10^{-4} Torr) at 100 °C and 150 °C, respectively.

Method D. A solution of SO_2Cl_2 (0.005 mmol) in dry toluene (0.5 mL) and solution of pyridine (0.01 mmol) or Me_2EtN (0.01 mmol) in dry toluene (0.5 mL) were added simultaneously dropwise (one drop every 3 s) to a stirred solution of precursor **2** (0.01 mmol) in dry toluene (10 mL) at −15 °C. The resulting dark green solution of **1** was passed through a jacketed Florisil column (6 × 1 cm) at −78 °C and washed with toluene using a low pressure of N_2. For isolation of radicals **1d** and **1e** an additional 1-cm layer of silica gel was placed on the bottom of the column. Solvents were removed under reduced pressure (~1 Torr) at temperatures below 0 °C to give a black-green solid of **1**.

X-ray Crystallography. Black-purple (**1d**) or black-green (**1e**) crystals (approximate dimensions 0.25 × 0.13 × 0.10 mm^3 for **1d** and 0.40 × 0.08 × 0.04 mm^3 for **1e**) were placed onto the tip of a 0.1-mm diameter glass fiber and mounted on a CCD diffractometer for data acquisition at 173(2) K. Preliminary sets of cell constants were calculated from reflections harvested from three sets of 50 (**1d**) or 20 (**1e**) frames. This produced initial orientation matrixes determined from 215 (**1d**) or 78 (**1e**) reflections. The data acquisitions were carried out using Mo Kα radiation (graphite monochromator, $\lambda = 0.71073$ Å) with frame durations of 60 (**1d**) or 120 (**1e**) seconds and a detector distance of 4.9 cm. Randomly oriented regions of reciprocal space were surveyed to the extent of one sphere and to a resolution of 0.84 Å. Four major sections of frames were collected with 0.30° (**1d**) or 0.50° (**1e**) steps in ω at four different ϕ settings and a detector position of −28° in 2θ. Final cell constants were calculated from 1617 (**1d**) or 2515 (**1e**) strong reflections from the actual data collection using SAINT V6.35A.[40] The intensity data for **1d** were corrected for absorption using TWINABS.[40] The intensity data for **1e** were corrected for absorption using SADABS.[41] Both structures were solved and refined using SHELXTL V6.12.[41] All non-hydrogen atoms were refined with anisotropic displacement parameters. All hydrogen atoms were placed in ideal positions and refined as riding atoms with relative isotropic displacement parameters.

The space group for **1d** was determined to be $C_{2/c}$ on the basis of systematic absence intensity statistics. The specimen selected for data collection was a nonmerohedral twin with the twin law [−1 0 −1.75/0 −1 0/0 0 1], which corresponds to a 180° rotation about direct axis (001).[40] Additional reflection manipulation was accomplished using program STRIP-REDUNDANT V1.1,[42] which removed redundant reflections. In addition, all systematic absence violations were removed using program SYSABSFILTER V1.1.[42] There were 4767 reflections associated solely with the major twin component, 4763 reflections associated solely with the minor twin component, and 6137 overlapping reflections.

The space group for **1e** was determined to be $P\bar{1}$; however its unit cell is coincidentally close to the reduced cell corresponding to a putative C-centered monoclinic cell. All three examined specimens of **1e** were pseudo-merohedral twins with the twin law (by rows) [1 0 0/0 1 0/0 1 −1]. All residuals for **1e** were in the range $R_1 = 0.085-0.090$.

Electrochemical Analysis. General Procedure. Cyclic voltametry was performed at ambient temperature using a CHI 660 electrochemical workstation (Austin TX) and a single-compartment microcell equipped with a 2-mm Pt disk working electrode, Pt wire counter electrode, and quasi-reference AgCl/Ag electrode. Dry and degassed CH_2Cl_2 or MeCN (2 mL) was transferred to a mixture of solid radical **1d** or **1e** (2 μmol) and 0.2 mmol of dry electrolytic grade [*n*-Bu_4N][ClO_4] (MeCN) or [*n*-Bu_4N][PF_6] (CH_2Cl_2) placed in an electrochemical microcell under Ar. Ar was passed through the resulting solution for 2 min. The electrochemical potential was scanned from −1.0 V to +1.4 V at a rate of 100 mV/s with respect to the quasi-reference AgCl/Ag electrode. At the end of the analysis a small amounts of ferrocene was added, and the potential was scanned again for referencing. Following a general procedure,[19] the Fc/Fc+ couple was set to +0.38 V relative to SCE in MeCN and +0.48V relative to SCE in CH_2Cl_2.

Stability Studies. General Procedure. Method A. Solid radical **1e** (0.01 mmol) was dissolved in dry benzene (10 mL), and the solution was degassed by three freeze/pump/thaw cycles and finally filled with Ar. The solution was transferred to an argon-filled UV cell equipped with a Teflon stopcock. For measurements in the presence of air, a part of the stock solution was placed in an ordinary UV cell, and air was slowly passed for 15 s. The samples were constantly irradiated with monochromatic light at 680 nm and the absorption at this wavelength was measured every 30 s at room temperature.

Method B. Solutions of radicals **1a**−**1c** in benzene were generated according to Method B using AgO (reaction times: 20 min, **1a**; 40 min, **1b**; **1c**, 75 min) and filtered through a microfilter. Solutions of **1d** and **1e** were prepared by dissolving sublimed radicals. The resulting solutions in ESR tubes (c = ~0.1 mM) were degassed by three freeze/pump/thaw cycles. One set of tubes was kept under vacuum, and the other was filled with dry Ar. Intensity of the ESR signal for each solution was monitored at room temperature for several days.

1,5,6,7,8-Pentachloro-3-phenylbenzo[1,2,4]thiadiazine[9] **(3e)**. A solution of freshly distilled SCl_2 (1.12 g, 11 mmol) in CH_2Cl_2 (10 mL) was added dropwise to a stirred

(39) Hammer, R. N.; Kleinberg, J.; Holtzclaw, H. F., Jr.; Johnson, K. W. R. *Inorg. Synth.* **1953**, *4*, 12−14.

(40) Bruker Analytical X-ray System, Madison, WI 2000.
(41) Bruker Analytical X-ray System, Madison, WI 2003.
(42) Brennessel, W. W.; Young, V. G., Jr. Unpublished results.

solution of crude *N*-chloro-*N*′-phenylbenzamidine (2.31 g), obtained from *N*-phenylbenzamidine (1.96 g, 10 mmol) and *tert*-butyl hypochlorite (1.19 g, 11 mmol) in CH_2Cl_2 (30 mL), and pyridine (1.58 g, 20 mmol) in CH_2Cl_2 (40 mL) at 0 °C.[11] Chlorine (about 50 mmol) was passed through the reaction mixture for 30 min. The mixture was stirred at 0 °C for 1 h and left overnight at ambient temperature. The resulting red precipitate was filtered to give 1.8 g (45% yield) of crude **3e**, which was used without further purification.

5,6,7,8-Tetrachloro-3-phenylbenzo[1,2,4]-4*H*-thiadiazine (2e). Crude sulfiminyl chloride **3e** (1.8 g, 4.5 mmol) was added in one portion to a stirred solution of dry 1-propanethiol (0.70 g, 9.2 mmol) in CH_2Cl_2 (50 mL) at ambient temperature. The reaction mixture was stirred for 20 min, diluted with CH_2Cl_2, and passed through a silica gel plug (CH_2Cl_2). Solvent was evaporated, and the organic products were passed through a short silica gel column using first a hexanes−CH_2Cl_2 mixture in 10:1 ratio to remove dipropyl disulfide and then in 1:1 ratio to elute **2e**, which after recrystallization (hexanes−toluene, 5:1 ratio) gave 1.38 g (84% yield) of a yellow solid: mp 193−195 °C; ^{1}H NMR (300 MHz, $CDCl_3$) δ 7.0 (brs, 1H), 7.42−7.55 (m, 3H), 7.62−7.65 (m, 2H); IR (neat) 3415 (N−H), 1626 (amidine), 1463 and 1349 (C_6Cl_4 ring) cm^{-1}; MS *m*/*e* (relative intensity) 364 (M^+, 2), 103 (100). Anal. Calcd for $C_{13}H_6Cl_4N_2S$: C, 42.89; H, 1.66; N, 7.69. Found: C, 42.76; H, 1.69; N, 7.57.

3-Phenylbenzo[1,2,4]-4*H*-thiadiazine-*S*-oxide (4a). A dark green solution of radical 3-phenylbenzo[1,2,4]thiadiazinyl (**1a**), prepared from **2a** (34 mg, 0.15 mmol) with Method C, was stirred at room temperature opened to air until the solution became colorless (approximately 3 h). Solvents were removed under reduced pressure, and the white solid residue was extracted on a filtration funnel with solvents of gradually increasing polarity starting with pentane. The main product (26 mg, 72% yield) was obtained from the fraction washed with CH_2Cl_2: mp >178 °C dec; ^{1}H NMR (300 MHz, DMSO-d_6) δ 7.45 (td, J_1 = 7.4, J_2 = 1.2 Hz, 1H), 7.60−7.70 (m, 6H), 7.78 (d, J = 7.5 Hz, 1H), 8.05−8.08 (m, 2H); IR (neat) 3245 and 3192 (N−H), 1031 (S=O) cm^{-1}; HRMS *m*/*e* calcd for $C_{13}H_{11}N_2OS$ 243.0592, found 243.0597.

5,6,7,8-Tetrachloro-3-phenylbenzo[1,2,4]-4*H*-thiadiazine-*S*-oxide (4e). The *S*-oxide was isolated in about 70% yield as the most polar colorless fraction (R_f ~0.35 in AcOEt) from a solid residue obtained after sublimation of **1e**: mp >247 °C dec; ^{1}H NMR (300 MHz, DMSO-d_6) δ 7.62−7.74 (m, 3H), 8.19−8.22 (m, 2H); IR (neat) 2814 (br N−H), 1055 (S=O) cm^{-1}; HRMS *m*/*e* calcd for $C_{13}H_6Cl_4N_2OS$ 377.8955, found 377.8940. Anal. Calcd for $C_{13}H_6Cl_4N_2OS$: C, 41.08; H, 1.59; N, 7.37. Found: C, 41.45; H, 1.63; N, 7.14.

Acknowledgment. Financial support for this work was received from the National Science Foundation (CHE-0096827). Collection of synchrotrone crystal data for **1e** was performed at ChemMatCARS Sector 15 of Argonne National Laboratory, which is principally supported by the National Science Foundation/Department of Energy (CHE0087817) and by the Illinois Board of Higher Education. The Advanced Photon Source is supported by the U.S. Department of Energy, Basic Energy Sciences, Office of Science, under Contract W-31-109-Eng-38. We thank Dr. David E. Cliffel for help with analysis of the electrochemical data.

Supporting Information Available: Kinetic analysis of the formation and decomposition curves for **1**, experimental, simulated, and difference spectra for **1**, spin densities, calculated hfcc, details of computational results, and full crystallographic results for **1d** and **1e** in CIF format. This material is available free of charge via the Internet at http://pubs.acs.org.

JO0486746